Velocity slip and temperature jump simulations by the three-dimensional thermal finite-difference lattice Boltzmann method

Minoru Watari*
LBM Fluid Dynamics Laboratory, 3-2-1 Mitahora-higashi, Gifu 502-0003, Japan
(Received 19 February 2009; published 19 June 2009)

Two problems exist in the current studies on the application of the lattice Boltzmann method (LBM) to rarefied gas dynamics. First, most studies so far are applications of two-dimensional models. The numbers of velocity particles are small. Consequently, the boundary-condition methods of these studies are not directly applicable to a multispeed finite-difference lattice Boltzmann method (FDLBM) that has many velocity particles. Second, the LBM and FDLBM share their origins with the Boltzmann equation. Therefore, the results of LBM and FDLBM studies should be verified by the results of the continuous Boltzmann equation. In my review to date on the LBM studies, it appears that such verifications were seldom done. In this study, velocity slip and temperature jump simulations in the slip-flow regime were conducted using a three-dimensional FDLBM model. The results were compared with preceding theoretical studies based on the continuous Boltzmann equation. The results agreed with the theory with errors of a few percent. To further improve the accuracy of the FDLBM, it seems necessary to increase the number of velocity particles.

DOI: 10.1103/PhysRevE.79.066706 PACS number(s): 47.11.−j, 47.45.−n, 51.10.+y

I. INTRODUCTION

Understanding rarefied gas dynamics is crucial in designing microelectromechanical systems [1]. Studies of the lattice Boltzmann method (LBM) and the finite-difference lattice Boltzmann method (FDLBM) as applied to rarefied gas dynamics started to appear recently [2–15].

The rarefied gas dynamics are represented properly by the Boltzmann equation. However, it is an equation in the six-dimensional (6D) phase space: three-dimensional (3D) velocity space plus 3D position space. In the LBM and FDLBM, substituting the velocity space by a limited number of velocity particles transforms the equations to 3D problems. It has been proved that the LBM and FDLBM are equivalent to the Navier-Stokes equations within the limits of a small Knudsen number. Therefore, in an intermediate flow, where both the continuity flow and the rarefied flow coexist, the LBM and FDLBM become ideal flow solvers if they can represent the rarefied gas flow properly.

The author has been studying multispeed FDLBM models [16–19] because the FDLBM has several advantages over the LBM. Multispeed thermal models are readily constructed because the selection of velocity particles is independent from the lattice configuration. The model can secure numerical stability by adjusting the time interval. A Nonuniform grid is available. This study started from the author's interest in knowing if the FDLBM can represent the rarefied gas flow properly.

The current studies of rarefied gas flows have two problems. First, most studies to date are applications of two-dimensional (2D) models and the numbers of velocity particles are small, therefore the boundary conditions are quite simple. The FDLBM models, especially 3D models, have many velocity particles and the boundary-condition methods of the previous rarefied gas studies are not directly applicable to these models.

Second, the LBM and FDLBM share their origins with the Boltzmann equation. Therefore, the results of LBM and FDLBM studies should be verified by the results of the continuous Boltzmann equation. In my review of LBM studies to date, it appears that such verifications were seldom done, although studies of the continuous Boltzmann equation have been carried out in depth and the data for verification are extensive.

This study applies the boundary-condition method to multispeed FDLBM thermal models and conducts velocity slip and temperature jump simulations using one of the author's FDLBM models. The simulation results are compared with those obtained from the continuous Boltzmann equation to verify how accurately the FDLBM can simulate rarefied gas flows and to identify the causes of the discrepancies.

II. RAREFIED GAS FLOW

This study focuses on a rarefied gas flow of Knudsen number K (the nondimensional parameter of the mean-free path divided by a characteristic length) of around 0.01–0.1, the so-called slip-flow regime. In this regime, in the vicinity of the wall, phenomena peculiar to a rarefied gas flow are observed. If the wall acts as a diffuse reflection boundary, velocity slip and temperature jump phenomena occur. These phenomena have been well understood since the 19th century, the era of Maxwell [20–23]. However, it was after World War II that the quantitative features were made clear. Many rarefied gas flow studies exist for the continuous Boltzmann equation [24–35]. In particular, there are many studies [24–31] of the Boltzmann equation with the BGK (Bhatnagar-Gross-Krook) collision term since the BGK formulation is easy to handle and still retains fundamental features of molecular gas dynamics. Therefore, the LBM and FDLBM, most of which are based on the BGK approximation, can be verified for their accuracy by comparing them with previous results. There are good references for rarefied

*watari-minoru@kvd.biglobe.ne.jp

 ©2009 The American Physical Society

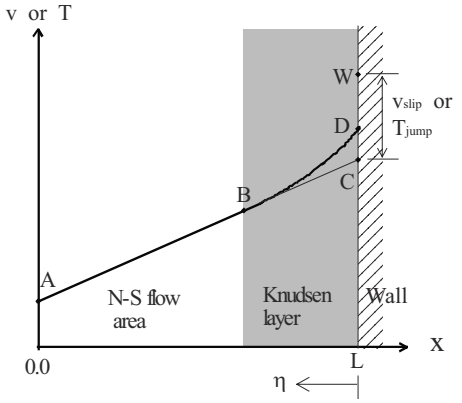

FIG. 1. Typical profile of velocity slip or temperature jump.

gas flows [36–41], of which the Sone and Aoki studies are the author's primary source.

Figure 1 depicts a typical velocity or temperature profile between parallel plates simulated in this paper. As the profile is antisymmetric, only half of it is shown. The lateral axis is an x position whereas the vertical axis corresponds to the velocity v along the y axis or the temperature T, depending on the velocity slip or temperature jump simulation.

The wall emits a local equilibrium distribution irrespective of the shape of the distribution injected into the wall. Consequently, the distribution of the gas on the wall is very distorted. This distorted distribution, moving away from the wall, is relaxed through particle collisions and approaches a quasiequilibrium state. The relaxation process, which is depicted as a portion B-D, occurs in a thin layer called the Knudsen layer. The thickness of the layer is of the order of the mean-free path.

A flow in the quasiequilibrium state is governed by continuity flow equations such as the Navier-Stokes equations. Therefore, we can call such an area the "N-S flow area." We know from the Navier-Stokes analysis that the velocity or temperature gradient is constant in a flow between parallel plates. The linear portion A-B, whose gradient is dv/dx or dT/dx, corresponds to the N-S flow area.

The gas velocity or temperature on the wall (point D) is inevitably less than the wall speed or the wall temperature (point W) because of the conservation of momentum or the conservation of energy.

The velocity slip v_{slip} and temperature jump T_{jump} are defined as the difference between the wall value (point W) and the cross point (point C) extended from the gradients in the N-S flow area. Knudsen profiles Δv and ΔT are the difference between the curved line B-D and the straight line B-C. According to Sone and Aoki, they are expressed (signs are changed from the original reference) as

$$\begin{bmatrix} v_{slip} \\ \Delta v \end{bmatrix} = \begin{bmatrix} 1.01619 \\ Y_0(\eta) \end{bmatrix} \frac{\sqrt{\pi}}{2} K \frac{dv}{dx}, \tag{1a}$$

$$\begin{bmatrix} T_{jump} \\ \Delta T \end{bmatrix} = \begin{bmatrix} 1.30272 \\ \Theta_1(\eta) \end{bmatrix} \frac{\sqrt{\pi}}{2} K \frac{dT}{dx}. \tag{1b}$$

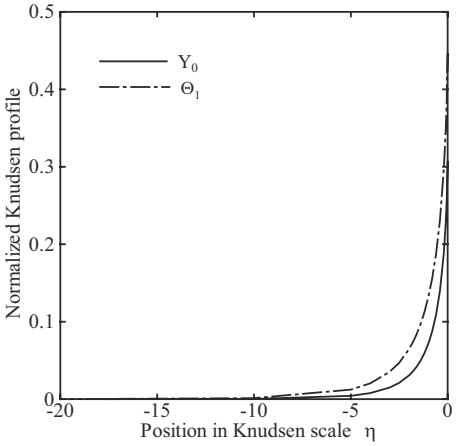

FIG. 2. Normalized Knudsen profiles under diffuse reflection boundary for the Boltzmann equation with BGK collision.

The functions $Y_0(\eta)$ and $\Theta_1(\eta)$ are shown in Fig. 2, where the variable η is a coordinate in the Knudsen layer measured normal to the wall and scaled by the Knudsen number

$$\eta = \frac{x - L}{\frac{\sqrt{\pi}}{2} K}. \tag{2}$$

III. THREE-DIMENSIONAL FDLBM MODEL

A 3D thermal model presented in Ref. [18] was chosen for the simulation studies. The evolution of the distribution function f_{ki} for the velocity particle $\mathbf{c}_{ki}$ is governed by the following equation:

$$\frac{\partial f_{ki}}{\partial t} + c_{ki\alpha} \frac{\partial f_{ki}}{\partial r_\alpha} = -\frac{1}{\tau}(f_{ki} - f_{ki}^{eq}), \tag{3}$$

where the variable t is time, r_α is the spatial coordinate, and τ is the relaxation-time constant. f_{ki}^{eq} is the local equilibrium distribution function. The subscript k indicates a group of the velocity particles whose speed is c_k and i indicates the direction of the particles. The subscript α indicates an x, y, or z component.

The macroscopic quantities of the density ρ, the velocity u_α, and the internal energy e are calculated from the distribution function

$$\rho = \sum_{ki} f_{ki}, \tag{4}$$

$$\rho u_\alpha = \sum_{ki} f_{ki} c_{ki\alpha}, \tag{5}$$

$$\rho\left(e + \frac{u^2}{2}\right) = \sum_{ki} f_{ki} \frac{c_k^2}{2}. \tag{6}$$

The pressure P, the temperature T, the ratio of specific heats γ, the speed of sound c_s, the viscosity coefficient μ, and the heat conductivity κ' have the following relationships:

$$P = \frac{2}{3}\rho e, \tag{7}$$

$$T = \frac{2e}{3}, \tag{8}$$

$$\gamma = \frac{5}{3}, \tag{9}$$

$$c_s = \sqrt{\gamma T}, \tag{10}$$

$$\mu = \frac{2}{3}\rho e \tau, \tag{11}$$

$$\kappa' = \frac{10}{9}\rho e \tau. \tag{12}$$

These are nondimensional quantities based on the reference density ρ_0, the reference length L, and the reference temperature T_0 (where R is the gas constant),

$$\rho, f_{ki}, f_{ki}^{eq} \quad \text{by} \quad \rho_0,$$

$$c_{ki\alpha}, u_\alpha, c_s, \bar{c} \quad \text{by} \quad \sqrt{RT_0},$$

$$e \quad \text{by} \quad RT_0,$$

$$T \quad \text{by} \quad T_0,$$

$$r_\alpha \quad \text{by} \quad L,$$

$$t, \tau \quad \text{by} \quad \frac{L}{\sqrt{RT_0}},$$

$$P \quad \text{by} \quad \rho_0 RT_0,$$

$$\mu, \kappa' \quad \text{by} \quad \rho_0 L\sqrt{RT_0}. \tag{13}$$

The local equilibrium distribution function f_{ki}^{eq} is written as follows:

$$f_{ki}^{eq} = \rho F_k \left[\left(1 - \frac{3u^2}{4e} + \frac{9u^4}{32e^2}\right) + \frac{3}{2e}\left(1 - \frac{3u^2}{4e}\right) c_{ki\xi} u_\xi + \frac{9}{8e^2}\left(1 - \frac{3u^2}{4e}\right) c_{ki\xi} c_{ki\eta} u_\xi u_\eta + \frac{9}{16e^3} c_{ki\xi} c_{ki\eta} c_{ki\zeta} u_\xi u_\eta u_\zeta + \frac{27}{128e^4} c_{ki\xi} c_{ki\eta} c_{ki\zeta} c_{ki\chi} u_\xi u_\eta u_\zeta u_\chi \right]. \tag{14}$$

The velocity particles $\mathbf{c}_{ki}$ consist of a rest particle and 4 speeds of 32 moving particles. The moving particles are obtained from the unit vectors in Table I multiplied by c_k.

The weighting coefficients F_k in the local equilibrium distribution function are

TABLE I. Unit vectors of moving particles, where $\varphi = \frac{1+\sqrt{5}}{2}$, $\lambda = \frac{1}{\sqrt{3}}$, and $\phi = \frac{\sqrt{2}}{\sqrt{5+\sqrt{5}}}$.

i:direction	Unit vector (c_{ix}, c_{iy}, c_{iz})
$i=1-8$	$\lambda(\pm 1, \pm 1, \pm 1)$
$i=9-12$	$\lambda(0, \pm \varphi^{-1}, \pm \varphi)$
$i=13-16$	$\lambda(\pm \varphi, 0, \pm \varphi^{-1})$
$i=17-20$	$\lambda(\pm \varphi^{-1}, \pm \varphi, 0)$
$i=21-24$	$\phi(0, \pm \varphi, \pm 1)$
$i=25-28$	$\phi(\pm 1, 0, \pm \varphi)$
$i=29-32$	$\phi(\pm \varphi, \pm 1, 0)$

$$F_0 = 1 - 32(F_1 + F_2 + F_3 + F_4), \tag{15a}$$

$$F_1 = \frac{1}{c_1^2(c_1^2 - c_2^2)(c_1^2 - c_3^2)(c_1^2 - c_4^2)} \times \left[\frac{35}{6}e^4 - \frac{35}{36}(c_2^2 + c_3^2 + c_4^2)e^3 + \frac{5}{24}(c_2^2 c_3^2 + c_3^2 c_4^2 + c_4^2 c_2^2)e^2 - \frac{c_2^2 c_3^2 c_4^2}{16}e \right], \tag{15b}$$

$$F_2 = \frac{1}{c_2^2(c_2^2 - c_3^2)(c_2^2 - c_4^2)(c_2^2 - c_1^2)} \times \left[\frac{35}{6}e^4 - \frac{35}{36}(c_3^2 + c_4^2 + c_1^2)e^3 + \frac{5}{24}(c_3^2 c_4^2 + c_4^2 c_1^2 + c_1^2 c_3^2)e^2 - \frac{c_3^2 c_4^2 c_1^2}{16}e \right], \tag{15c}$$

$$F_3 = \frac{1}{c_3^2(c_3^2 - c_4^2)(c_3^2 - c_1^2)(c_3^2 - c_2^2)} \times \left[\frac{35}{6}e^4 - \frac{35}{36}(c_4^2 + c_1^2 + c_2^2)e^3 + \frac{5}{24}(c_4^2 c_1^2 + c_1^2 c_2^2 + c_2^2 c_4^2)e^2 - \frac{c_4^2 c_1^2 c_2^2}{16}e \right], \tag{15d}$$

$$F_4 = \frac{1}{c_4^2(c_4^2 - c_1^2)(c_4^2 - c_2^2)(c_4^2 - c_3^2)} \times \left[\frac{35}{6}e^4 - \frac{35}{36}(c_1^2 + c_2^2 + c_3^2)e^3 + \frac{5}{24}(c_1^2 c_2^2 + c_2^2 c_3^2 + c_3^2 c_1^2)e^2 - \frac{c_1^2 c_2^2 c_3^2}{16}e \right]. \tag{15e}$$

There is an arbitrariness in the selection of moving particle speeds c_k. In the original paper [18], $(c_1, c_2, c_3, c_4) = (1.0, 2.0, 3.0, 4.0)$ was assumed.

In the BGK formulation, the Knudsen number is defined by the relaxation-time constant and the average particle speed $\bar{c}$,

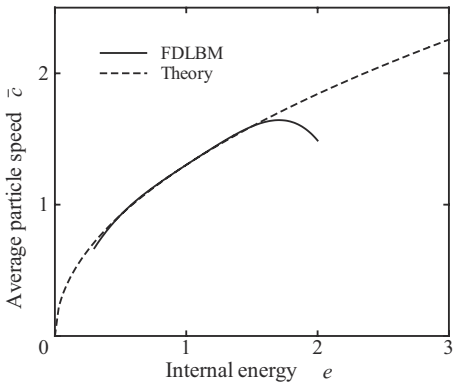

FIG. 3. Nondimensional average particle speed of the FDLBM model and the theoretical value.

$$K = \tau \bar{c}. \tag{16}$$

Theoretically the average particle speed is

$$\bar{c} = \sqrt{\frac{16}{3\pi}e}. \tag{17}$$

The arbitrariness in the selection of c_k was utilized to make the FDLBM average particle speed fit the theoretical value. The FDLBM average particle speed was calculated using the equilibrium distribution with $u_\alpha = 0.0$,

$$\rho \bar{c} = \sum_{ki} f_{ki}^{eq} c_k. \tag{18}$$

The speeds c_k were determined to give the best match around $e = 1.0$. The following equations were solved numerically:

$$\bar{c} \text{ by FDLBM} = \bar{c} \text{ by theory at } e = 0.5, 1.0, 1.5,$$

$$\frac{\partial \bar{c}}{\partial e} \text{ by FDLBM} = \frac{\partial \bar{c}}{\partial e} \text{ by theory at } e = 1.0. \tag{19}$$

The result $(c_1, c_2, c_3, c_4) = (0.818, 1.642, 2.592, 3.800)$ was obtained. The comparison of the average particle speed between the FDLBM and the theory is shown in Fig. 3.

IV. NUMERICAL SIMULATIONS

The velocity slip and temperature jump were examined by simulating flows between parallel plates (Fig. 4). In the simulation, the internal energy e was used instead of the temperature T and the symbol v was used to express the velocity u_y. The plates were placed at $x = \pm 1.0$.

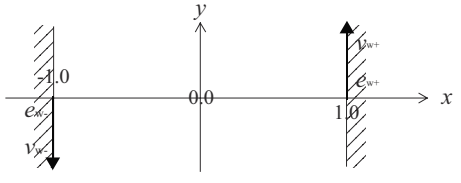

FIG. 4. A flow between parallel plates. In the velocity slip simulation $v_w = \pm 0.01$ and $e_w = 1.0$. In the temperature jump simulation $v_w = 0.0$ and $e_w = 1.0 \pm 0.01$.

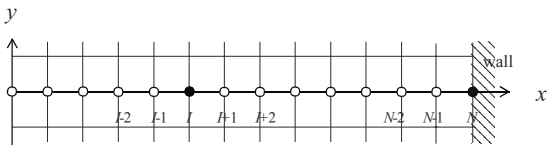

FIG. 5. Nodes for the spatial derivative calculation.

In the velocity slip simulation, the plates moved with constant speed ($v_w = \pm 0.01$) in opposite directions along the y axis. The internal energies of both plates were kept at the same constant value ($e_w = 1.0$). In the temperature jump simulation, the plates were at rest ($v_w = 0.0$) but the internal energies were kept at different values ($e_w = 1.0 \pm 0.01$).

The evolution Eq. (3) was solved by a finite-difference equation,

$$f_{ki}^{new} = f_{ki} - c_{kix}\frac{\partial f_{ki}}{\partial x}\Delta t - \frac{1}{\tau}(f_{ki} - f_{ki}^{eq})\Delta t. \tag{20}$$

For the spatial derivative $\partial f_{ki}/\partial x$, the second-order upwind scheme was applied as far as possible to suppress numerical viscosity. The derivative at position I is calculated as follows (see Fig. 5):

$$\frac{\partial f_{ki}}{\partial x} = \begin{cases} \dfrac{3f_{ki,I} - 4f_{ki,I-1} + f_{ki,I-2}}{2\Delta x} & \text{if } c_{kix} \geq 0 \\ \dfrac{3f_{ki,I} - 4f_{ki,I+1} + f_{ki,I+2}}{-2\Delta x} & \text{if } c_{kix} < 0. \end{cases} \tag{21}$$

For $c_{kix} \geq 0$, the evolution Eq. (20) with Eq. (21) was applied up to the wall ($I = N$).

For $c_{kix} < 0$ on the wall ($I = N$), since the wall is a diffuse reflection boundary, the distribution is a local equilibrium distribution $f_{ki}^{eq}(\rho_w, v_w, e_w)$ determined from the wall condition: the velocity v_w and the internal energy e_w. The density ρ_w is determined so as to give a zero-mass flow normal to the wall, where $f_{ki,N}$ is the incident distribution at $I = N$,

$$\sum_{c_{kix}>0} f_{ki,N}c_{kix} + \sum_{c_{kix}<0} f_{ki}^{eq}(\rho_w, v_w, e_w)c_{kix} = 0. \tag{22}$$

The density ρ_w was easily calculated because the density is a linear factor in the equilibrium distribution function,

$$\rho_w = -\frac{\sum_{c_{kix}>0} f_{ki,N}c_{kix}}{\sum_{c_{kix}<0} f_{ki}^{eq}(\rho_w = 1.0, v_w, e_w)c_{kix}}. \tag{23}$$

For $c_{kix} < 0$ in the gas region ($I < N$), the evolution Eq. (20) was applied. However, at the node $I = N-1$, the second-order upwind scheme is not applicable. The first-order upwind scheme was applied there,

$$\frac{\partial f_{ki}}{\partial x} = \frac{f_{ki,N-1} - f_{ki,N}}{-\Delta x}. \tag{24}$$

For $c_{kix} < 0$ and $I \leq N-2$, the evolution Eq. (20) with the second-order upwind Eq. (21) was applied.

The relaxation-time constant was varied as $\tau = 0.01, 0.05, 0.1$ to realize various Knudsen numbers. The

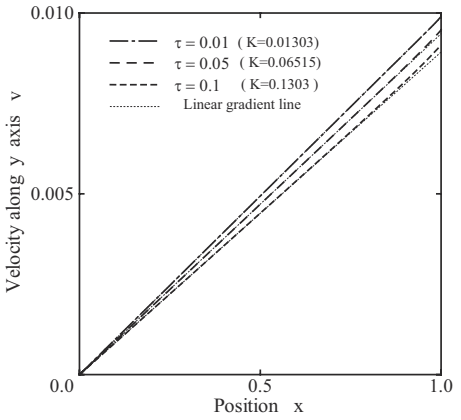

FIG. 6. Velocity profiles for various relaxation-time constants (Knudsen numbers).

mesh size $\Delta x=0.005$ (or $N=200$) was common. However, the time increment Δt was changed according to the relaxation-time constant to ensure numerical stability: $\Delta t=0.00025$ for $\tau=0.01$ and $\Delta t=0.0004$ for $\tau=0.05,0.1$.

V. SIMULATION RESULTS

Velocity profiles in a steady state in the velocity slip simulation for $\tau=0.01,0.05,0.1$ $(K=0.01303,0.06515,0.1303)$ are shown in Fig. 6. Linear gradient lines were drawn applying the least square method to the portion of the N-S flow area. The velocity slip was obtained as the difference between the wall speed $(v_w=0.01)$ and the speed where the linear gradient line intercepts the wall. The velocity slip divided by the velocity gradient $v_{slip}/\frac{dv}{dx}$ versus the Knudsen number is shown in Fig. 7.

The velocity residues Δv from the velocity gradient lines were obtained to depict the Knudsen profile. They are shown in Fig. 8. If they are normalized according to the theoretical relationship (1a) and (2),

$$\frac{\Delta v}{\frac{\sqrt{\pi}}{2}K\frac{dv}{dx}} \text{ vs } \frac{x-1.0}{\frac{\sqrt{\pi}}{2}K}, \tag{25}$$

they are gathered into a single curve as shown in Fig. 9 with the theoretical Knudsen profile $Y_0(\eta)$.

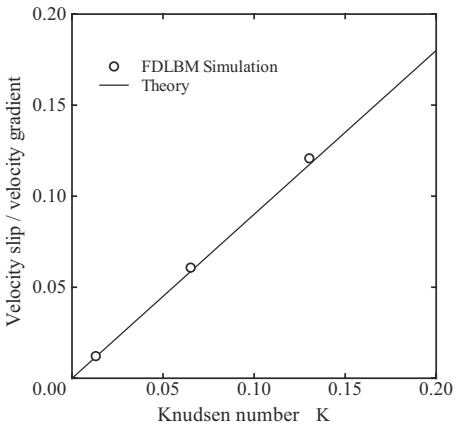

FIG. 7. Velocity slip divided by the velocity gradient $v_{slip}/\frac{dv}{dx}$ versus Knudsen number.

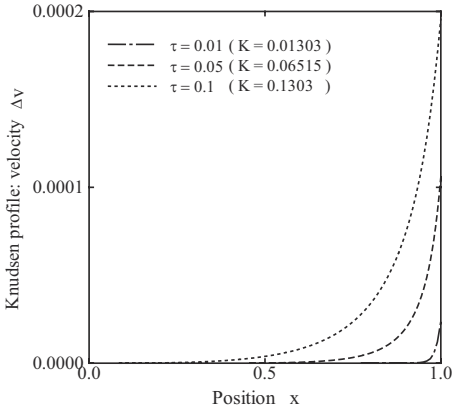

FIG. 8. Knudsen profiles: velocity residues from the velocity gradient lines.

Internal energy profiles in a steady state in the temperature jump simulation for various τ are shown in Fig. 10. The internal energy jump divided by the internal energy gradient $e_{jump}/\frac{de}{dx}$ versus the Knudsen number is shown in Fig. 11.

The Knudsen profiles Δe are shown in Fig. 12. If they are normalized according to the theoretical relationship (1b)and (2),

$$\frac{\Delta e}{\frac{\sqrt{\pi}}{2}K\frac{de}{dx}} \text{ vs } \frac{x-1.0}{\frac{\sqrt{\pi}}{2}K}, \tag{26}$$

they are gathered into a single curve as shown in Fig. 13 with the theoretical Knudsen profile $\Theta_1(\eta)$.

The velocity slip and temperature jump in the FDLBM simulation show good agreement with the theoretical values. The error in the velocity slip is 3.5% and the error in the temperature jump is 2%. The Knudsen profiles in the velocity slip and the temperature jump coincide with the theoretical profiles.

VI. DISCUSSION

This section discusses how the velocity slip and the temperature jump are determined in the FDLBM simulation. As

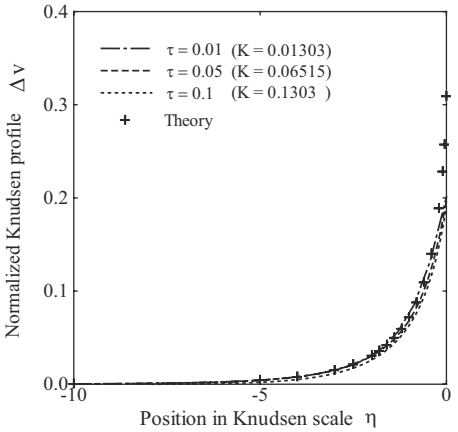

FIG. 9. Normalized Knudsen profile versus position in Knudsen scale.

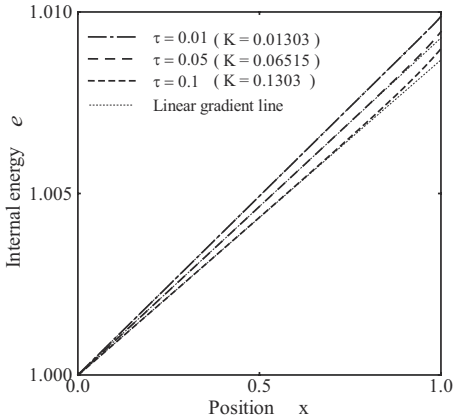

FIG. 10. Internal energy profiles for various relaxation-time constants (Knudsen numbers).

the wall is a diffuse reflection boundary, irrespective of the shape of the distribution $f_{ki,N},(c_{kix}>0)$ injected into the wall, the wall emits a local equilibrium distribution $f_{ki}^{eq}(\rho_w,v_w,e_w)$ for $c_{kix}<0$. The density ρ_w is determined so that the mass flow normal to the wall M_x^{wall} is zero,

$$M_x^{wall}=\sum_{c_{kix}>0} f_{ki,N}c_{kix}+\sum_{c_{kix}<0} f_{ki}^{eq}(\rho_w,v_w,e_w)c_{kix}=0. \quad (27)$$

Consequently, the distribution of the gas on the wall is very distorted. The distribution for $c_{kix}>0$ is streamed from the gas region, whereas the distribution for $c_{kix}<0$ is a local equilibrium. There is a discontinuity at the plane of $c_{kix}=0$. This distorted distribution, on moving from the wall, is relaxed through particle collisions and approaches a quasiequilibrium state in the N-S flow area.

The distribution f_{ki} is divided into a local equilibrium part f_{ki}^{eq} and a nonequilibrium part f_{ki}^{ne},

$$f_{ki}=f_{ki}^{eq}+f_{ki}^{ne}. \quad (28)$$

In the N-S flow area in a steady state, a convection process and a collision process are balanced,

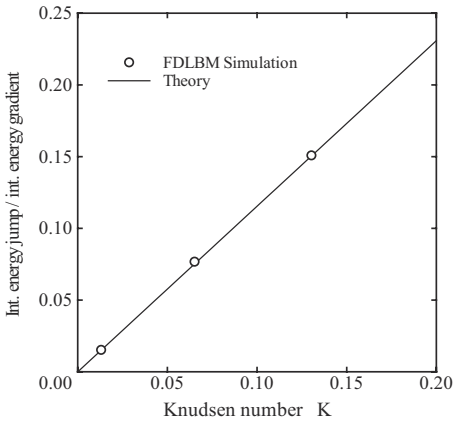

FIG. 11. Internal energy jump divided by the internal energy gradient $e_{jump}/\frac{de}{dx}$ versus Knudsen number.

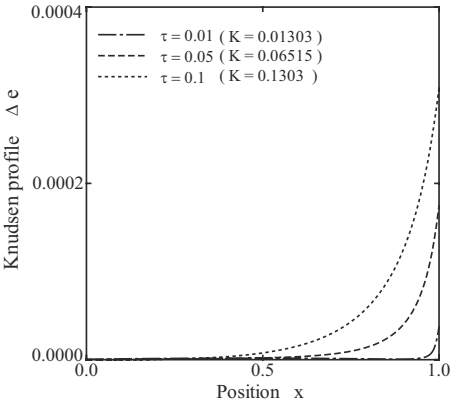

FIG. 12. Knudsen profiles: internal energy residues from the internal energy gradient lines.

$$c_{ki\alpha}\frac{\partial f_{ki}}{\partial r_\alpha}=-\frac{1}{\tau}(f_{ki}-f_{ki}^{eq}). \quad (29)$$

Consequently, the nonequilibrium part f_{ki}^{ne} is expressed

$$f_{ki}^{ne}=-\tau c_{kix}\frac{\partial f_{ki}}{\partial x}\cong-\tau c_{kix}\frac{\partial f_{ki}^{eq}}{\partial x}$$

$$=-\tau c_{kix}\frac{dv}{dx}\frac{\partial f_{ki}^{eq}}{\partial v}, \quad (30a)$$

$$=-\tau c_{kix}\frac{de}{dx}\frac{\partial f_{ki}^{eq}}{\partial e}. \quad (30b)$$

The y momentum flow P_{xy} along the x axis and the internal energy flow S_x along the x axis are given by

$$P_{xy}=\sum_{ki} f_{ki}c_{kix}c_{kiy}, \quad (31a)$$

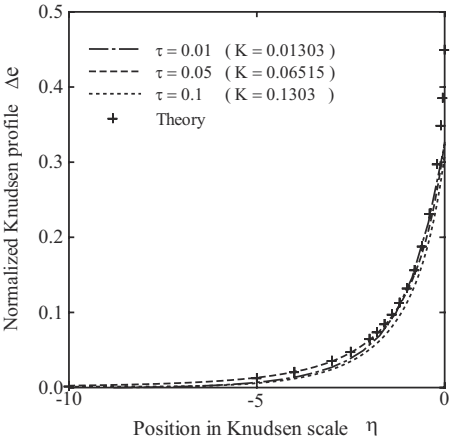

FIG. 13. Normalized Knudsen profile versus position in Knudsen scale.

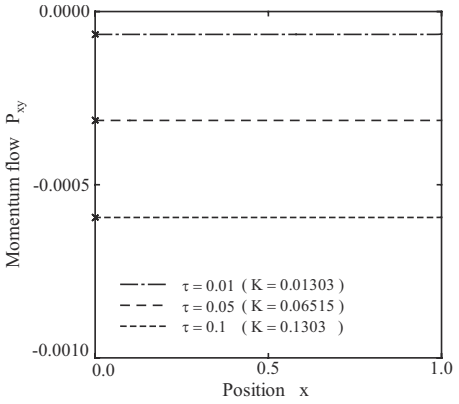

FIG. 14. Momentum flow obtained from the simulation. Symbols × are the values in the N-S flow area calculated using Eq. (32).

$$S_x = \sum_{ki} f_{ki} \frac{c_k^2}{2} c_{kix}. \tag{31b}$$

Since the contributions by f_{ki}^{eq} on P_{xy} and S_x are zero, if the expression (30) is substituted into Eq. (31), P_{xy} and S_x are expressed as follows in the N-S flow area,

$$P_{xy}^{NS} = -\frac{2}{3}\rho e \tau \frac{dv}{dx} = -\mu \frac{dv}{dx}, \tag{32a}$$

$$S_x^{NS} = -\frac{10}{9}\rho e \tau \frac{de}{dx} = -\kappa' \frac{de}{dx}. \tag{32b}$$

Figures 14 and 15 show P_{xy} and S_x obtained from the simulations based on Eq. (31). The symbols × are the values in the N-S flow area, calculated using Eq. (32) with the dv/dx or de/dx values obtained in the simulations.

From the conservation of momentum and energy, P_{xy} and S_x are constant from the N-S flow area, through the Knudsen layer, up to the wall.

If we divide P_{xy} and S_x into two parts with the flows to the right and left,

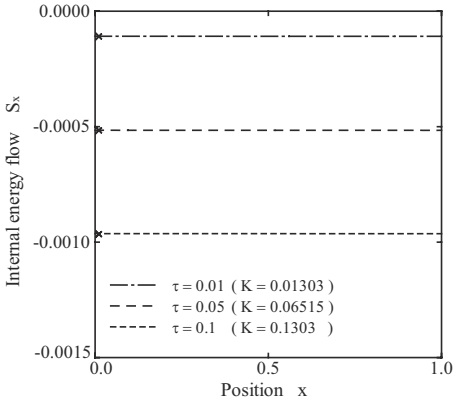

FIG. 15. Internal energy flow obtained from the simulation. Symbols × are the values in the N-S flow area calculated using Eq. (32).

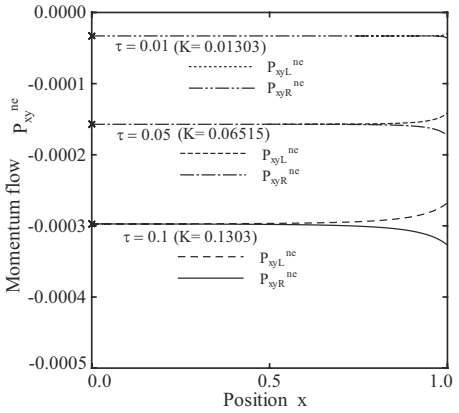

FIG. 16. Momentum flow by nonequilibrium part obtained from the simulation. Symbols × are the values in the N-S flow area calculated using Eq. (30).

$$P_{xy} = P_{xy}^{ne} = P_{xyR}^{ne} + P_{xyL}^{ne} = \sum_{c_{kix}>0} f_{ki}^{ne} c_{kix} c_{kiy} + \sum_{c_{kix}<0} f_{ki}^{ne} c_{kix} c_{kiy}, \tag{33a}$$

$$S_x = S_x^{ne} = S_{xR}^{ne} + S_{xL}^{ne} = \sum_{c_{kix}>0} f_{ki}^{ne} \frac{c_k^2}{2} c_{kix} + \sum_{c_{kix}<0} f_{ki}^{ne} \frac{c_k^2}{2} c_{kix}, \tag{33b}$$

then in the N-S flow area, Eq. (30) indicates that f_{ki}^{ne} is constant and antisymmetric regarding c_{kix}. Consequently, $P_{xyR}^{ne} = P_{xyL}^{ne}$ and $S_{xR}^{ne} = S_{xL}^{ne}$ in the N-S flow area.

Figures 16 and 17 show P_{xyR}^{ne}, P_{xyL}^{ne} and S_{xR}^{ne}, S_{xL}^{ne} obtained from the simulations based on Eq. (33). The symbols × are the values in the N-S flow area, calculated using Eq. (30) with the dv/dx or de/dx values obtained in the simulations. These figures demonstrate how the distorted distributions given at the wall are relaxed in the Knudsen layer.

Next, the momentum flow P_{xy}^{wall} and the energy flow S_x^{wall} on the wall are considered,

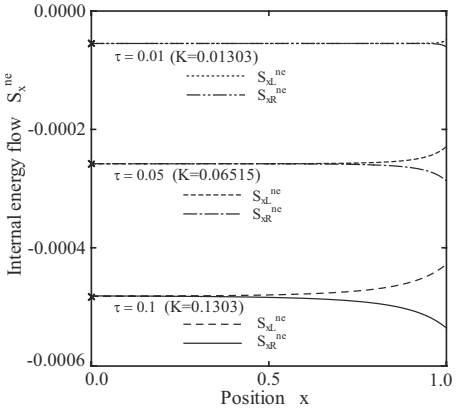

FIG. 17. Internal energy flow by nonequilibrium part obtained from the simulation. Symbols × are the values in the N-S flow area calculated using Eq. (30).

TABLE II. Comparison of dv/dx between the simulation and the calculated value based on Maxwell's assumption.

τ	Simulation	Maxwell's assumption
0.01	0.00988	0.00989
0.05	0.00943	0.00948
0.1	0.00892	0.00901

$$P_{xy}^{wall} = \sum_{c_{kix}>0} f_{ki,N} c_{kix} c_{kiy} + \sum_{c_{kix}<0} f_{ki}^{eq}(\rho_w, v_w, e_w) c_{kix} c_{kiy}, \tag{34a}$$

$$S_x^{wall} = \sum_{c_{kix}>0} f_{ki,N} \frac{c_k^2}{2} c_{kix} + \sum_{c_{kix}<0} f_{ki}^{eq}(\rho_w, v_w, e_w) \frac{c_k^2}{2} c_{kix}. \tag{34b}$$

The gas velocity and internal energy on the wall (point D) are inevitably less than the wall values (point W) if the conservation of momentum and energy is considered. The velocity slip and temperature jump have close relationships with the gradients in the N-S flow area. If the gradients increase, so do P_{xy} and S_x, therefore, the velocity slip and the temperature jump must increase to balance the incoming P_{xy} and S_x.

To understand this relationship, we consider, for example, an approximation of the velocity slip, in which the incident distribution is assumed to be a N-S distribution extending to the wall. This assumption aims to solve the problem at the point C instead of D. In fact, this assumption was adopted by Maxwell and gives a good estimate as long as the Knudsen number is small.

$$f_{ki,N} = f_{ki}^{eq} + f_{ki}^{ne} = f_{ki}^{eq}(\rho, v_c, e) - \tau c_{kix} \frac{dv}{dx} \frac{\partial f_{ki}^{eq}}{\partial v},$$

$$v_c = \frac{dv}{dx} \times 1. \tag{35}$$

Simultaneous equations of $M_x^{wall}=0$ and $P_{xy}^{wall}=P_{xy}^{NS}$ are solved under assumption (35). The comparison of the dv/dx between the simulation result and the calculated based on Maxwell's assumption is shown in Table II. As expected, Maxwell's assumption approaches the simulation as τ (or K) becomes smaller (the point C approaches the point D).

As we have seen so far, the FDLBM appears to be fundamentally right, however, it still has errors of a few percent. The author believes that the number of velocity particles is not large enough to express the boundary conditions at the wall. For example, particles of $c_{kix}=0$ do not contribute any effect on Eqs. (27) and (34), although they represent a range of particles in the shallow angles to the wall.

To understand this effect, the following moments pointing to half space were calculated using the FDLBM equilibrium distribution function,

TABLE III. Comparison of the moment contributions pointing to half space between the theory and the FDLBM.

Moment	Theory	FDLBM
M_{xR}	0.3257	0.3113 (0.951)
P_{xyR}	0.003257	0.003033 (0.931)
S_{xR}	0.4343	0.4149 (0.955)

$$M_{xR} = \sum_{c_{kix}>0} f_{ki}^{eq} c_{kix}, \quad P_{xyR} = \sum_{c_{kix}>0} f_{ki}^{eq} c_{kix} c_{kiy},$$

$$S_{xR} = \sum_{c_{kix}>0} f_{ki}^{eq} \frac{c_k^2}{2} c_{kix}. \tag{36}$$

They were compared with the theoretical values. The boldface variable $d\mathbf{c}$ represents a 3D volume element $(dc_x dc_y dc_z)$,

$$M_{xR} = \int_{c_x>0} f^{eq} c_x d\mathbf{c}, \quad P_{xyR} = \int_{c_x>0} f^{eq} c_x c_y d\mathbf{c},$$

$$S_{xR} = \int_{c_x>0} f^{eq} \frac{c^2}{2} c_x d\mathbf{c}, \tag{37}$$

where

$$f^{eq} = \rho \left(\frac{3}{4\pi e} \right)^{3/2} \exp\left[-\frac{3}{4e} (c_\alpha - u_\alpha)^2 \right]. \tag{38}$$

$\rho=1.0$, $e=1.0$, and $u_\alpha=0.0$, but for P_{xyR} $u_y=0.01$, were assumed. The results are shown in Table III. The parenthesized values are the ratios to the theoretical values. The FDLBM show smaller values by several percent. The author believes the ratio will approach unity if the number of velocity particles is increased, consequently, the accuracy of FDLBM simulation will be further improved. The author has just started a study using a 2D model to clarify the relationship between the number of velocity particles and the accuracy of FDLBM.

VII. CONCLUSIONS

Velocity slip and temperature jump simulations in the slip-flow regime were conducted using a 3D FDLBM model. The results were compared with theoretical studies based on the continuous Boltzmann equation and were checked to see if the FDLBM possesses fundamental properties of rarefied gas flows.

(1) The velocity slip and temperature jump in the FDLBM simulation showed good agreement with the theory. The error in the velocity slip is 3.5% and the error in the temperature jump is 2%.

(2) The Knudsen profiles: the residues of velocity and temperature in the Knudsen layer coincided with the theoretical profiles.

(3) The FDLBM simulation proved a fundamental

property: the momentum flow or the energy flow is constant from the N-S flow area, through the Knudsen layer, and up to the wall.

(4) The FDLBM simulation proved a fundamental property: the flow in the N-S flow area is in a quasiequilibrium state.

(5) The manner in which the distorted distribution given at the wall is relaxed in the Knudsen layer was demonstrated.

(6) The manner in which the velocity slip or the temperature jump is determined in the FDLBM simulation was clarified.

(7) To improve the accuracy of the FDLBM rarefied gas flow simulation, it seems necessary to increase the number of velocity particles.

[1] G. E. Karniadakis and A. Beskok, *Micro Flows: Fundamentals and Simulation* (Springer, New York, 2000).
[2] C. Y. Lim, C. Shu, X. D. Niu, and Y. T. Chew, Phys. Fluids **14**, 2299 (2002).
[3] X. Nie, G. D. Doolen, and S. Chen, J. Stat. Phys. **107**, 279 (2002).
[4] M. Sbragaglia and S. Succi, Phys. Fluids **17**, 093602 (2005).
[5] S. Ansumali and I. V. Karlin, Phys. Rev. E **66**, 026311 (2002).
[6] G. H. Tang, W. Q. Tao, and Y. L. He, Phys. Fluids **17**, 058101 (2005).
[7] Y. Zhang, R. Qin, and D. R. Emerson, Phys. Rev. E **71**, 047702 (2005).
[8] Z. W. Tian, C. Zou, H. J. Liu, Z. L. Guo, Z. H. Liu, and C. G. Zheng, Physica A **385**, 59 (2007).
[9] Y. H. Zhang, X. J. Gu, W. Barber, and D. R. Emerson, EPL **77**, 30003 (2007).
[10] X. D. Niu, C. Shu, and Y. T. Chew, Int. J. Mod. Phys. C **16**, 1927 (2005).
[11] X. D. Niu, S. A. Hyodo, T. Munekata, and K. Suga, Phys. Rev. E **76**, 036711 (2007).
[12] V. Sofonea and R. F. Sekerka, Phys. Rev. E **71**, 066709 (2005).
[13] V. Sofonea and R. F. Sekerka, J. Comput. Phys. **207**, 639 (2005).
[14] V. Sofonea, Phys. Rev. E **74**, 056705 (2006).
[15] V. Sofonea, Europhys. Lett. **76**, 829 (2006).
[16] M. Watari and M. Tsutahara, Phys. Rev. E **67**, 036306 (2003).
[17] M. Watari and M. Tsutahara, Phys. Rev. E **70**, 016703 (2004).
[18] M. Watari and M. Tsutahara, Physica A **364**, 129 (2006).
[19] M. Watari, Physica A **382**, 502 (2007).
[20] E. H. Kennard, *Kinetic Theory of Gases* (McGraw-Hill, New York, 1938).
[21] J. C. Maxwell, Philos. Trans. R. Soc. London **157**, 49 (1867).
[22] J. C. Maxwell, Philos. Trans. R. Soc. London **170**, 231 (1879).
[23] R. A. Millikan, Phys. Rev. **21**, 217 (1923).
[24] Y. Sone, *Rarefied Gas Dynamics*, edited by L. Trilling and H. Y. Wachman (Academic, New York, 1969), p. 243.
[25] Y. Sone, *Rarefied Gas Dynamics*, edited by D. Dini (Editrice Tecnico Scientifica, Pisa, 1971), p. 737.
[26] Y. Sone, J. Phys. Soc. Jpn. **21**, 1620 (1966).
[27] Y. Sone, J. Phys. Soc. Jpn. **21**, 1836 (1966).
[28] Y. Onishi, Trans. Jpn. Soc. Aeronaut. Space Sci. **17**, 93 (1974).
[29] Y. Onishi, Trans. Jpn. Soc. Aeronaut. Space Sci. **17**, 151 (1974).
[30] Y. Sone and Y. Onishi, J. Phys. Soc. Jpn. **35**, 1773 (1973).
[31] Y. Sone and Y. Onishi, J. Phys. Soc. Jpn. **44**, 1981 (1978).
[32] Y. Sone, T. Ohwada, and K. Aoki, Phys. Fluids A **1**, 1398 (1989).
[33] Y. Sone, T. Ohwada, and K. Aoki, Phys. Fluids A **1**, 363 (1989).
[34] T. Ohwada, Y. Sone, and K. Aoki, Phys. Fluids A **1**, 1588 (1989).
[35] T. Ohwada, Y. Sone, and K. Aoki, Phys. Fluids A **1**, 2042 (1989).
[36] H. Grad, Commun. Pure Appl. Math. **2**, 331 (1949).
[37] C. Cercignani, *Theory and Application of the Boltzmann Equation* (Scottish Academic, Edinburgh, 1975).
[38] Y. Sone and K. Aoki, *Molecular Gas Dynamics* (Asakura, Tokyo, 1994) (in Japanese).
[39] Y. Sone, Annu. Rev. Fluid Mech. **32**, 779 (2000).
[40] K. Aoki, in Proceedings of 39th AIAA Aerospace Sciences Meeting and Exhibit, 2001 (unpublished), paper 2001–0874.
[41] Y. Sone, *Molecular Gas Dynamics* (Birkhäuser, Boston, 2002).